

# VLA OH Zeeman Observations of the star forming region S88B

A. P. Sarma<sup>1</sup>, C. L. Brogan<sup>2</sup>, T. L. Bourke<sup>3</sup>, M. Eftimova<sup>1,4</sup>, T. H. Troland<sup>5</sup>

## ABSTRACT

We present observations of the Zeeman effect in OH thermal absorption main lines at 1665 and 1667 MHz taken with the Karl G. Jansky Very Large Array (VLA) toward the star forming region S88B. The OH absorption profiles toward this source are complicated, and contain several blended components toward a number of positions. Almost all of the OH absorbing gas is located in the eastern parts of S88B, toward the compact continuum source S88B-2 and the eastern parts of the extended continuum source S88B-1. The ratio of 1665/1667 MHz OH line intensities indicates the gas is likely highly clumped, in agreement with other molecular emission line observations in the literature. S88-B appears to present a similar geometry to the well-known star forming region M17, in that there is an edge-on eastward progression from ionized to molecular gas. The detected magnetic fields appear to mirror this eastward transition; we detected line-of-sight magnetic fields ranging from 90-400  $\mu\text{G}$ , with the lowest values of the field to the southwest of the S88B-1 continuum peak, and the highest values to its northeast. We used the detected fields to assess the importance of the magnetic field in S88B by a number of methods; we calculated the ratio of thermal to magnetic pressures, we calculated the critical field necessary to completely support the cloud against self-gravity and compared it to the observed field, and we calculated the ratio of mass to magnetic flux in terms of the critical value of this parameter. All these methods indicated that the magnetic field in S88B is dynamically significant, and should provide an important source of support against gravity. Moreover, the magnetic energy density is in approximate equipartition with the turbulent energy density, again pointing to the importance of the magnetic field in this region.

---

<sup>1</sup>Physics Department, DePaul University, 2219 N. Kenmore Ave., Byrne Hall 211, Chicago IL 60614; asarma@depaul.edu

<sup>2</sup>National Radio Astronomy Observatory, Charlottesville, VA 22903

<sup>3</sup>Harvard-Smithsonian Center for Astrophysics, Cambridge, MA 02138

<sup>4</sup>Current Address: Dept. of Physics & Astronomy, University of North Carolina, Chapel Hill, NC 27599

<sup>5</sup>Dept. of Physics & Astronomy, University of Kentucky, Lexington KY 40506

*Subject headings:* H II regions — ISM: clouds — ISM: individual (S88B) — ISM: kinematics and dynamics — ISM: magnetic fields — ISM: molecules

## 1. INTRODUCTION

Massive stars affect the structure and dynamics of galaxies, the planet formation process, and even the formation of low mass stars via outflows, winds, and supernova explosions that drive mixing and turbulence in the interstellar medium (e.g., Zinnecker & Yorke 2007, and references therein). Yet, our understanding of their formation and evolution remains unclear. Moreover, the importance of magnetic fields in the formation of stars, both low and high mass, has long been acknowledged (e.g., Mouschovias 1987; Heiles et al. 1993; Crutcher 1999; McKee 1999). Indeed, ongoing theoretical work continues to probe the effects of magnetic fields on the star formation process (e.g., Zhao et al. 2011; Mellon & Li 2009; Boss 2007; Shu et al. 2006; Mouschovias et al. 2006; Nakamura & Li 2005). However, observational data on magnetic fields is still scarce and theoretical work is hampered by the lack of information on magnetic field strengths in different density regimes.

With these considerations in view, we have observed the high mass star forming region S88B with the Karl G. Jansky Very Large Array (VLA) for the Zeeman effect in thermal absorption lines of OH at 1665 and 1667 MHz. Observations of the Zeeman effect in absorption lines with interferometers like the VLA provide an excellent method of *mapping* the magnetic field in regions that are along the line of sight toward strong background continuum sources (e.g., Brogan & Troland 2001; Sarma et al. 2000). In the next subsection, we will present some details of the source S88B. In § 2, we present details of the observations and reduction of the data. The results are presented in § 3, and discussed in § 4. In § 5, we state our conclusions.

### 1.1. S88B

S88B is a high mass star forming region (near  $l = 61^{\circ}48, b = 0^{\circ}09$ ) with a bolometric luminosity of  $9.0 \times 10^4 L_{\odot}$  (Mueller et al. 2002). It has been observed at a wide variety of wavelengths. There is some confusing nomenclature in the literature, and so we begin by discussing the morphology of its surroundings. S88 is itself a diffuse extended nebula, and is likely a very evolved H II region (e.g., Felli & Harten 1981). About  $14'$  to its southeast lie two bright knots of optical nebulosity: S88A and S88B (e.g., see the red Palomar Sky Survey print in Fig. 1 of Evans et al. 1981). No radio continuum emission is observed from

the western source, S88A. Strong radio emission is observed from an H II region centered slightly to the east of the optical nebulosity S88B, and this is the target source for our Zeeman observations. Felli & Harten (1981) first proposed that the radio source in S88B was composed of two components, based on their 5 GHz continuum observations. The more extended component to the west (e.g., see § 3.1, and Fig. 1 in this paper) that intersects the optical nebulosity is S88B-1, whereas the compact component to the east is S88B-2. In their high resolution 6 cm VLA image (HPBW 0.4"), Wood & Churchwell (1989) resolved out many details of these two sources — what they call G61.48+0.09A is referenced as S88B-2 in this paper (and most of the literature), whereas their source G61.48+0.09B is a group of low intensity sources to the southwest of S88B-1. Following Evans et al. (1981), we adopt the distance to S88B of 2.0 kpc. More recently, Sewilo et al. (2004) have claimed a distance of  $4.1 \pm 2.4$  kpc to S88B on the basis of their H110 $\alpha$  recombination line and H<sub>2</sub>CO absorption observations; we note that our adopted value is within their error limits. Moreover, Goetz et al. (2003) have estimated on the basis of foreground star counts that the distance to S88B cannot be substantially greater than 2.0 kpc.

## 2. OBSERVATIONS & DATA REDUCTION

The observations were carried out with the Very Large Array (VLA) of the NRAO<sup>1</sup> in 2003 in the B-configuration, and combined with C-configuration data observed in 1997. Important parameters of the observations are listed in Table 1. Both circular polarizations and both main lines (1665 and 1667 MHz) of OH were observed simultaneously in absorption. In order to mitigate instrumental effects, a front-end transfer switch was used to alternate the sense of circular polarization passing through each telescope’s IF system every  $\sim 10$  minutes.

The editing, calibration, Fourier transformation, deconvolution, and calculation of optical depths for the OH data were carried out using the Astronomical Image Processing System (AIPS) of the NRAO. Following standard procedure for Zeeman effect observations, bandpass correction was applied only to the Stokes *I* data set, since bandpass effects subtract out to first order in the Stokes *V* data, and the bandpass correction process adds noise to the *V* profiles. The B and C configuration data were combined in the uv-plane using the AIPS task *DBCON*. The rms in the continuum image of the combined B and C configuration data is 0.8 mJy beam<sup>-1</sup>, whereas the rms in a channel of the line data is 1.7 mJy beam<sup>-1</sup>. Magnetic fields were determined as described in § 3.3 by using the Multichannel Image Re-

---

<sup>1</sup>The National Radio Astronomy Observatory (NRAO) is a facility of the National Science Foundation operated under cooperative agreement by Associated Universities, Inc.

construction, Image Analysis and Display (MIRIAD) software processing package, formerly of the Berkeley-Illinois-Maryland Array (BIMA) and now incorporated into the Combined Array for Research in Millimeter-Wave Astronomy (CARMA) telescope.

### 3. RESULTS

#### 3.1. The 18 cm Continuum

Figure 1 shows our highest resolution 18 cm continuum image of S88B made with uniform weighting (beam HPBW  $3''.1 \times 3''.0$ ). The extended western component S88B-1 and the compact component on the eastern side S88B-2, first identified by Felli & Harten (1981), are clearly visible in this figure. We determined the integrated flux for S88B-1 to be  $4.27 \pm 0.23$  Jy, and the integrated flux for S88B-2 to be  $0.79 \pm 0.32$  Jy. In a 5 GHz continuum survey with the NRAO 140-ft telescope (HPBW  $6''.5$ ), Reifenstein et al. (1970) obtained 6.1 Jy for the source  $61.5+0.1$  which is a combination of S88B-1 and S88B-2. In a 12-hr synthesis map with Westerbork (WSRT) at 5 GHz (HPBW  $6''.6$ ), Felli & Harten (1981) obtained a total flux density of  $6.1 \pm 0.2$  Jy for S88B. At 4.9 GHz, Garay et al. (1993) measured 4.4 Jy toward S88B-1 and 0.8 Jy toward S88B-2 in a combined C and D configuration observation with the VLA (HPBW  $\sim 4''$ ). The integrated flux densities measured with these shorter wavelength data are in good agreement with the 18 cm VLA results, suggesting that the emission is predominantly either near the turnover point or optically thin ( $\alpha = -0.1$ ,  $S_\nu \propto \nu^\alpha$ ). Figure 2 shows the  $350 \mu\text{m}$  dust continuum image of Mueller et al. (2002) superposed on our 18 cm continuum image, along with other pertinent information — these are discussed in § 4.1.

#### 3.2. OH Absorption

The OH absorption profiles toward S88B are complicated, with several blended components toward a number of positions. In order to characterize the velocity structure, optical depth profiles for the OH lines were calculated with the AIPS task *COMB* using standard procedure (e.g., see Roberts, Crutcher, & Troland 1995). The OH column density was then determined using the relation

$$N_{\text{OH}}/T_{\text{ex}} = C \int \tau_v dv \quad \text{cm}^{-2} \text{ K}^{-1} \quad (1)$$

where  $T_{\text{ex}}$  is the excitation temperature of OH and the constant  $C = 4.1063 \times 10^{14}$  and  $2.2785 \times 10^{14} \text{ cm}^{-2} (\text{km s}^{-1})^{-1}$  for the OH 1665 and 1667 MHz lines respectively (Crutcher 1977).

The optical depth profiles reveal complex kinematics with a number of heavily blended components present toward much of the region. In order to highlight the prominent absorption components, contour plots of the OH optical depth in several velocity channels are shown in Figure 3, superposed on a grayscale image of the 18 cm continuum. Every third velocity channel is displayed, and the plots are shown over the velocity range  $17.4 \text{ km s}^{-1}$  to  $24.0 \text{ km s}^{-1}$ . Figure 4 shows plots of  $N(\text{OH})/T_{\text{ex}}$  toward S88B at 1667 MHz. In principle, variations in  $N(\text{OH})/T_{\text{ex}}$  may arise due to variations in the OH column density, or due to variations in  $T_{\text{ex}}$ , or both. However, in the results and discussion, we quote only variations in  $N(\text{OH})/T_{\text{ex}}$ , since the excitation temperature cannot be measured based on absorption studies alone. Further discussion about possible variations in  $T_{\text{ex}}$  appears in § 4.1.

From Figures 3 and 4, we identified four prominent absorption enhancements, and these are marked in Figure 4 as OH-a, OH-b, OH-c, and OH-d respectively. The absorption enhancement OH-a lies to the southwest of the continuum peak of S88B-1; it is seen in the  $19.1 \text{ km s}^{-1}$  panel in Figure 3, with a peak  $\tau \sim 0.5$ . OH-a is also seen in the  $19.9 \text{ km s}^{-1}$  panel of Figures 3 with a higher peak  $\tau \sim 1$ . In this  $19.9 \text{ km s}^{-1}$  panel, we also see the enhancements OH-b and OH-c, the former to the northwest of the continuum peak of S88B-1, and the latter about midway between S88B-1 and S88B-2. Finally, OH-d is seen in the  $20.7$ ,  $21.5$ , and  $22.4 \text{ km s}^{-1}$  panels of Figure 3, with high peak  $\tau \sim 2$  in two of these panels; it lies northward of the S88B-2 continuum peak; OH-d is also visible at the highest velocities at which OH absorption is observed ( $\sim 23 \text{ km s}^{-1}$ ). The high  $\tau$ 's in OH-d account for the peak in  $N(\text{OH})/T_{\text{ex}}$  to the north of the continuum peak of S88B-2.

### 3.3. Magnetic Field Strengths

The magnetic field strengths in S88B were determined using the Zeeman effect, by fitting a numerical frequency derivative of the Stokes  $I$  spectrum to the Stokes  $V$  spectrum for each pixel in the absorption line cube. The Stokes parameters have the standard definition of  $I = (\text{RCP} + \text{LCP})$ , and  $V = (\text{RCP} - \text{LCP})$ ; RCP is right- and LCP is left-circular polarization; RCP has the standard radio definition of clockwise rotation of the electric vector when viewed along the direction of wave propagation. Since the observed  $V$  spectrum may also contain a scaled replica of the  $I$  spectrum itself, the Stokes  $V$  spectral profile can be described by the equation (Troland & Heiles 1982; Sault et al. 1990):

$$V = aI + \frac{b}{2} \frac{dI}{d\nu} \quad (2)$$

In this equation, the fit parameter  $a$  represents the scaled-down replica of the  $I$  profile in the  $V$  profile;  $a$  is usually the result of small calibration errors in  $\text{RCP}$  vs.  $\text{LCP}$ ; for all results

reported here,  $a \leq 10^{-3}$ . For thermally excited lines such as the OH 1665 and 1667 MHz lines reported in this paper,  $b = zB \cos \theta$ , where  $B$  is the magnetic field,  $\theta$  is the angle of the magnetic field to the line of sight, and  $z$  is the Zeeman splitting factor which is equal to  $z = 3.27 \text{ Hz } \mu\text{G}^{-1}$  for the 1665 MHz line of OH, and  $1.96 \text{ Hz } \mu\text{G}^{-1}$  for the 1667 MHz line of OH (Kazes & Crutcher 1986). We determined magnetic field strengths in S88B by using a least-squares method to fit equation (2) to the Stokes  $V$  spectra to solve for  $a$  and  $b$ . The results of the fits give the line-of-sight component of the magnetic field,  $B_{\text{los}} = B \cos \theta$ . It is usual practice to consider the results to be significant only if the derived value of  $B_{\text{los}}$  is greater than the  $3\sigma$  level. For Zeeman effect observations in OH absorption lines, we usually impose a stronger condition — we consider the detections to be significant only if both 1665 and 1667 MHz  $B_{\text{los}}$  values are greater than the  $3\sigma$  level. In the current observations, however, this stronger criterion for significance would leave out some important information on the field. Toward S88B-2, the 1665 MHz profiles show a  $\sim 200 \mu\text{G}$  field with about  $5\sigma$  level of significance, whereas the 1667 MHz profiles show a field below the  $3\sigma$  level. Therefore, for S88B-2 only, we have relaxed the criterion above to consider the measurement to be significant if it displays a  $3\sigma$  detection only in the 1665 MHz line. We believe this is reasonable, since the measured value of  $B_{\text{los}}$  toward this source does not appear to be wildly discrepant from the measured value toward S88B-1. The non-detection at 1667 MHz toward S88B-2 is not surprising. The 1667 MHz Stokes  $V$  signal is weaker than the 1665 MHz Stokes  $V$  signal because the Zeeman splitting factor for OH 1667 MHz lines ( $z = 1.96 \text{ Hz } \mu\text{G}^{-1}$ ) is less than that for OH 1665 MHz lines ( $z = 3.27 \text{ Hz } \mu\text{G}^{-1}$ ). This inequality in the Zeeman factors would not impact the result as much if the OH gas was thermalized and homogenous, since the intensity ratios would then be  $\tau_{67}/\tau_{65} = 9/5$ . However, as described below (§ 4.1),  $\tau_{67}/\tau_{65} = 1.0 - 1.3$  toward S88B, which makes the sensitivity of the 1667 MHz line to the Zeeman effect less than that of the 1665 MHz line.

The resulting  $B_{\text{los}}$  map (taken from the 1665 MHz data) is shown in Figure 5. In the area enclosed by the thick-lined ellipse in this figure, the detected field is above the  $3\sigma$  level only in the 1665 MHz line, whereas in the rest of the displayed  $B_{\text{los}}$  map, the field is above the  $3\sigma$  level in both 1665 and 1667 MHz lines, with peak signal-to-noise ratios of  $\sim 10$ . Examples of the Stokes  $I$  and  $V$  profiles together with the derivative of  $I$  scaled by the fitted value of  $B_{\text{los}}$  are shown in Figure 6 and Figure 7; the locations toward which these profiles have been plotted are marked in Figure 5 by a “+” and a “×” respectively. From Figure 6 and Figure 7, it is evident that the magnetic field is detected in the component with  $v_{\text{LSR}} \sim 21 \text{ km s}^{-1}$ ; no fields were detected in any of the other velocity components. Toward S88B-1, we see from Figure 5 that  $B_{\text{los}}$  increases from about  $90 \mu\text{G}$  in the southwest to about  $400 \mu\text{G}$  in the northeast; this is the case in both 1665 and 1667 MHz lines. Meanwhile, toward S88B-2, the 1665 MHz line reveals values of  $B_{\text{los}}$  as high as  $\sim 270 \mu\text{G}$ .



## 4. DISCUSSION

### 4.1. Morphology and Kinematics

Early optical, radio, and infrared observations of S88B by Pipher et al. (1977) revealed that the peak of the near infrared (NIR) position is eastward of the optical nebula, whereas the radio continuum peak is even farther to the east than the NIR peak. This eastward progression is consistent with our observation of the location of the absorbing OH gas. It is clear from Figure 3 that almost all of the OH absorbing gas is located in the eastern half of S88B (i.e., all of S88B-2, and the eastern part of the extended source S88B-1). We did not detect any OH absorption in the western parts of S88B-1, where it is coincident with the H $\alpha$  nebulosity. The molecular cloud associated with S88B was mapped by Evans et al. (1981) in several CO transitions at low resolution (HPBW 1'–2'), and found to extend over 10' (6.5 pc) with a total mass of  $5 \times 10^3 M_{\odot}$ . Evans et al. (1981) speculated that the H II regions S88B-1 and S88B-2 are a blister formation in the molecular cloud which we are observing from the side. The velocities of the absorbing OH gas match up well with molecular line velocities; e.g., the CO lines are singly peaked at 21 km s $^{-1}$  (Evans et al. 1981). Moreover, recombination line observations by Garay et al. (1994) with the VLA (HPBW  $\sim 2''$ ) revealed that the center velocity of the single-peaked H92 $\alpha$  line emission toward S88B-1 increases from 22 km s $^{-1}$  at the eastern edge of S88B-1 to 32 km s $^{-1}$  at the western edge. The 22 km s $^{-1}$  velocity in the H92 $\alpha$  recombination line at the eastern edge of S88B-1 matches well with the OH absorption data — e.g., see the panels between 21.5 km s $^{-1}$  and 22.4 km s $^{-1}$  in Figure 3. On the other hand, the recombination line velocity at the western edge matches well with the optical H $\alpha$  velocities which exceed 28 km s $^{-1}$  (Deharveng & Maucherat 1978). In other words, we are observing an edge-on transition from the ionized gas to the molecular gas in S88B, similar to M17 (Brogan & Troland 2001).

While the velocity structure of OH absorption observed by us toward S88B is complicated, the highest values for  $N(OH)/T_{\text{ex}}$  are to the north of the continuum peak S88B-2. While this may, in principle, be due to variations in  $N(OH)$  or  $T_{\text{ex}}$  or both, other tracers indicate that the column of absorbing gas is indeed greater in the eastern parts of S88B (i.e., toward S88B-2). Toward the H $\alpha$  peak in the west, Felli & Harten (1981) found a relatively low  $A_v = 5$  mag. Based on their observations of IR fine structure lines, Herter et al. (1982) measured  $A_v = 26 \pm 9$  mag at the position of the 2.2 NIR  $\mu\text{m}$  peak. This 2.2  $\mu\text{m}$  peak was resolved by Deharveng et al. (2000) into a system of three stars (82, 83, 84) located on the eastern edge of the optical nebulosity — their positions are marked in Figure 2. In contrast, toward S88B-2 in the east, Goetz et al. (2003) found  $A_v \sim 70$  mag by comparing their observed Br $\alpha$  flux with 5 GHz radio continuum data from the literature. S88B-2 also coincides with the 350  $\mu\text{m}$  dust continuum peak from Mueller et al. (2002), as shown in

Figure 2. There is also an extension in the 350  $\mu\text{m}$  dust continuum image to the northwest, which coincides with the location of S88B-1 (Fig. 2). In fact, due to the high obscuration toward the eastern parts of S88B, a complete census of the exciting/ionizing stars of S88B-1 and S88B-2 has proved impossible so far. Deharveng et al. (2000) suggested that star 82 could be the ionizing/exciting source of S88B-1, based on its high luminosity and central location (see Fig. 2), but admitted the likelihood that other stars also contribute to the excitation/ionization in the region. Other possible candidates for exciting sources are the stars L1 (for S88B-2) and L2 (for S88B-1), detected by Puga et al. (2004) at a near-infrared wavelength of 3.5  $\mu\text{m}$  ( $L'$ -band) and marked in Figure 2; however, the issue remains open because Puga et al. (2004) could not determine the spectral type of L1 or L2 as they did not detect them in their J, H, or  $K'$  near-infrared bands.

If the absorbing OH gas is thermalized and homogenous (i.e., not clumpy within the observing beam), the ratio of the optical depths of the 1665 MHz and 1667 MHz lines should be  $\tau_{67}/\tau_{65} = 9/5 = 1.8$ . However, the observed profiles toward S88B do not show this ratio. Instead, observed ratios  $\tau_{67}/\tau_{65}$  are in the range 1.0-1.3 over most parts of the source. While it is likely that the excitation temperatures for the two lines at 1665 MHz and 1667 MHz are not the same, it is unlikely that this difference would cancel out the expected ratio of optical depths over the whole source. More likely, the OH gas is clumped on size scales smaller than the beam. Such clumpiness has been found also in molecular emission lines. The CO  $J=2-1$  and  $^{13}\text{CO}$   $J=2-1$  and  $J=1-0$  data (HPBW 22''-33'') of White & Fridlund (1992) reveal a horseshoe-like structure surrounding the optical nebulosity, which they ascribe to material excited along the periphery of an outflow cavity that encloses the optical nebula. Indeed, Phillips & Mampaso (1991) have reported a low collimation bipolar outflow extending over 3' from their CO observations; this CO outflow was also observed by Ridge & Moore (2001). Both the CO and  $^{13}\text{CO}$  images in White & Fridlund (1992) show highly fragmented structure, in agreement with the clumpy structure suggested by the OH absorption observations. More evidence of clumping comes from observations of  $\text{NH}_3$  lines at high angular resolution (HPBW 4'') with the VLA by Gomez et al. (1995). They found compact ammonia structures with sizes of 0.2 pc toward both S88B-1 and S88B-2. They suggest that these ammonia clumps correspond to compact molecular structures embedded within the larger molecular cloud, and that these clumps have been heated by the radiation from the star(s) that ionize(s) the associated H II regions. Finally, recent  $\text{C}^{18}\text{O}$  observations by Saito et al. (2007) with a beam HPBW of 15'' provide additional evidence of clumpy structure (also see § 4.2.1 below); their clump B is marked in Figure 2.

The OH excitation temperature  $T_{\text{ex}}$  (which will be required in the calculations below) cannot be measured based on absorption studies alone, but reasonable limits for it can be set from our observations, and a likely value estimated based on other tracers. The



minimum continuum  $S_\nu$  against which the line is detected is  $\sim 10$  mJy beam $^{-1}$  — we can use this to set an upper limit on  $T_{\text{ex}}$ . Using  $S_\nu \rightarrow T_{\text{b}} : 1$  mJy beam $^{-1} \rightarrow 17$  K, we get an upper limit of 170 K for  $T_{\text{ex}}$ . It is also unlikely that  $T_{\text{ex}}$  is less than the typical dark cloud value of 10 K. Estimates of the kinetic temperature from other molecular tracers are also relevant if we assume LTE. From observations of the (2,2) and (3,3) lines of  $\text{NH}_3$ , Gomez et al. (1995) found  $T_{\text{kin}} = 80$  K toward S88B-1 (their western  $\text{NH}_3$  clump) and 70 K toward S88B-2 (their eastern  $\text{NH}_3$  clump). Based on CO observations, White & Fridlund (1992) estimated  $T_{\text{kin}} \sim 60$  K. Chini et al. (1986) found a dust temperature for S88B equal to  $T_{\text{dust}} = 42$  K. Mozurkewich, Schwartz, & Smith (1986) fitted a 2-component dust model for S88B, and obtained  $T_{\text{dust}} = 40$  K and 116 K. The higher  $T_{\text{d}}$  may be due to compact embedded sources or it may reflect an enhanced population of small grains (Wu & Evans 1989). Indeed, Jourdain de Muizon et al. (1990) have reported observations of PAH emission features toward S88B. Mueller et al. (2002) found  $T_{\text{dust}} = 75$  K from their 350  $\mu\text{m}$  dust continuum observations. We adopt  $T_{\text{ex}} = 60$  K for our calculations, but note that  $T_{\text{ex}}$  likely varies over the source; still, it must lie between 10-170 K.

## 4.2. Magnetic Fields

Our observations of the Zeeman effect in OH absorption lines at 1665 and 1667 MHz have yielded  $B_{\text{los}}$  values in the range of 90 to 400  $\mu\text{G}$ . These values are typical of magnetic fields in molecular clouds detected via the Zeeman effect in the density regimes accessible via H I and OH thermal lines, as tabulated in Crutcher (1999). Note, however, that our detected fields are higher than the single dish measurements by Crutcher et al. (1987), who found  $B_{\text{los}} = 69 \pm 5$   $\mu\text{G}$  toward S88B with the Nancay single dish. This is expected, since the low angular resolution (HPBW  $3'.5 \times 19'$ ) of Nancay will cause fields to be averaged over a large area, leading to much lower  $B_{\text{los}}$  values.

### 4.2.1. Magnetic Field Energetics

The magnetic field in a cloud may consist of a static component  $B_{\text{s}}$ , and a time-dependent or wave component  $B_{\text{w}}$ . The static component connects the cloud to the external medium and determines the total magnetic flux throughout the cloud, but it can only provide support to the cloud perpendicular to the field lines. The wave component is associated with MHD waves in the cloud, and it can provide three dimensional support to the cloud. In principle, the observed  $B_{\text{los}}$  may consist of contributions from each of these two components. In reality, however, the Zeeman effect likely traces the strength of the static component of

the magnetic field only. This is because spatial averaging over the beam and along the line of sight tends to cancel the contribution from the wave component (e.g., Brogan & Troland 2001, and references therein). A principal goal of Zeeman effect measurements, therefore, is to estimate the importance of the magnetic field to the dynamics and evolution of star forming regions like S88B. As summarized in Crutcher (1999), such estimates also require other physical parameters such as internal velocity dispersion, hydrogen column density, and radius, to be known.

The relevant physical parameters mentioned above for estimating the importance of the magnetic field are available either from the present observations of S88B or from the literature. First, we must decide on an appropriate value for the radius. The highest resolution molecular line emission observations available to date are the  $C^{18}O$  observations of Saito et al. (2007) referred to above (with beam HPBW  $15''$ ). Clumps B, C, and D in their observations all have radius  $\sim 0.2$  pc. Therefore, we adopt  $r = 0.2$  pc for the radius in all the following calculations. Next, the hydrogen column density can be estimated from the OH line data, subject to certain assumptions. We use an average value of  $N_{OH}/T_{ex} = 6.0 \times 10^{14} \text{ cm}^{-2} \text{ K}^{-1}$  (see Fig. 4). For the excitation temperature, we use  $T_{ex} = 60$  K, based on the discussion in § 4.1 above. Then, to get  $N_{H_2}$ , we use the conversion ratio  $N_{H_2}/N_{OH} = 2 \times 10^6$  from Roberts et al. (1995) for S106. This makes the OH abundance a factor of 10 greater than that in dark clouds found by Crutcher (1979). Note, however, that if we consider the standard conversion ratio  $N_{H_2}/A_v \sim 10^{21}$ , and use  $A_v = 70$  mag for S88B (see § 4.1 above), we obtain  $N_{H_2}/N_{OH} = 1.9 \times 10^6$ , which justifies our use of the Roberts et al. (1995) value rather than the dark cloud value; similar results were found for M17 by Brogan & Troland (2001). Using this conversion ratio, we get  $N_{H_2} = 7.2 \times 10^{22} \text{ cm}^{-2}$ . This gives a hydrogen density  $n(H_2) = 1.7 \times 10^5 \text{ cm}^{-3}$ , which compares well with the value of  $n(H_2) = 1.51 \times 10^5 \text{ cm}^{-3}$  found by Saito et al. (2007) for the clump designated as *B* in their  $C^{18}O$  observations (see Fig. 2). It is worth noting here that at lower resolution (HPBW  $30''$ ), Phillips & Mampaso (1991) determined a mean  $n(H_2) \sim 6 \times 10^3 \text{ cm}^{-3}$ . Together, this is further proof of the clumping in S88B discussed in 4.1 above, since the larger beam filling factor in a higher angular resolution observation of a clumpy region will naturally give a larger value for the density. Note, however, that the density cannot be substantially greater than  $\sim 10^5 \text{ cm}^{-3}$ , a conclusion reached by Phillips et al. (1988) based on the absence of  $H_2CO$  emission (Evans et al. 1981) toward S88B. Other parameters of interest are the velocity dispersion (which can be obtained from the observed line width) and the magnetic field; the adopted values for the average observed line width of OH lines and the average  $B_{los}$  in S88B are listed in Table 2. For the calculations below, we will follow Crutcher (1999), and use total (static) magnetic field strength equal to 2 times  $B_{los}$ .

We can now proceed to assess the importance of the magnetic field in S88B, using a

number of approaches. First, we consider the parameter  $\beta_p$ , which is the ratio of thermal to magnetic pressures (Crutcher 1999); it is a crucial parameter in any theory or simulation of the structure and evolution of molecular clouds that incorporates magnetic fields. If  $\beta_p < 1$ , then magnetic fields are important; the lower the value of  $\beta_p$ , the more dominant is the magnetic field. Based on the adopted values in Table 2, we find  $\beta_p = 0.14$  in S88B, indicating the importance of the magnetic field in this region. Our value for  $\beta_p$  in S88B is similar to that in high mass star forming regions like DR 21 OH 1, where  $\beta_p = 0.21$ , and W3 (main), where  $\beta_p = 0.13$  (Crutcher 1999, and references therein). Another way to assess the importance of the magnetic field in S88 is to use the relation

$$B_{S, \text{crit}} = 5 \times 10^{-21} N_p \quad \mu\text{G}, \quad (3)$$

where  $N_p$  is the average proton column density in the cloud. Equation 3 is a result of equating the static magnetic energy of the cloud to its gravitational energy;  $B_{S, \text{crit}}$  is then the average static magnetic field in the cloud that would completely support it against self-gravity. If the actual static magnetic field in the cloud  $B_S > B_{S, \text{crit}}$ , then the cloud can be completely supported by the magnetic field, and is said to be magnetically subcritical. Further evolution of the cloud perpendicular to the field lines will occur primarily via ambipolar diffusion. The field can be judged to be dynamically important to the region even if it is less than  $B_{S, \text{crit}}$ , but is comparable to it. For  $N_{\text{H}_2} = 7.2 \times 10^{22} \text{ cm}^{-2}$  from Table 2 above, we get  $B_{S, \text{crit}} = 700 \mu\text{G}$ . Our average total (static) magnetic field strength ( $= 2$  times  $B_{\text{los}}$  in Table 2) is  $400 \mu\text{G}$ ; that is, the observed magnetic field strength is within a factor of  $\sim 2$  less than the critical field. Therefore, the magnetic field should be dynamically significant, providing an important source of support against self gravity. Yet another parameter to judge the extent to which a static magnetic field can support a cloud against gravitational collapse is the observed mass to magnetic flux ratio  $[M/\Phi_B]$ , defined by Crutcher (1999) in units of the critical value. This is equivalent to the consideration of  $B_{S, \text{crit}}$ , and may be redundant here, but we state it nevertheless to express our results in this alternative language. If the ratio of observed  $[M/\Phi_B]$  to the critical value is greater than 1, then the region is magnetically supercritical, meaning that the magnetic field cannot by itself provide support against gravitational collapse. For S88B, we find the observed  $[M/\Phi_B]$  in units of the critical value to be 1.8. This is consistent with observations to date; Crutcher (1999) found the observed  $[M/\Phi_B]$  in terms of the critical value to have an average value equal to 2 in a summary of available Zeeman measurements in molecular clouds. The calculated value for S88B indicates that whereas the static magnetic field by itself is not enough to support the molecular cloud against gravitational collapse, it is high enough to provide a significant source of support. Perhaps more important, however, in a highly supersonic medium like the S88B molecular cloud, is that for the magnetic field to be important, its energy density must be comparable to, or greater than, the turbulent energy density. The supersonic nature

of the medium is clear from the value of the sonic Mach number  $m_s$  given in Table 3; from it, we have that the ratio of the one-dimensional velocity dispersion ( $\sigma$ ) to the isothermal sound speed ( $c_s$ ) in S88B is  $\sigma/c_s = 2.3$ . This is a common result in molecular clouds; in his compilation of results for 27 molecular clouds, Crutcher (1999) found that motions are supersonic by about a factor of 5. Table 3 also lists the Alfvénic Mach number ( $m_A$ ) to be equal to 1. This implies that the magnetic energy density is comparable to the turbulent energy density, that is, these two energies are in approximate equipartition.

Finally, we can use the measured  $B_{\text{los}}$  to assess the relative importance of the gravitational, kinetic, and magnetic energy terms  $\mathcal{W}$ ,  $\mathcal{T}$ , and  $\mathcal{M}$ , in the virial equation (McKee et al. 1993). To calculate their values, we use the expressions for  $\mathcal{W}$ ,  $\mathcal{T}$ , and  $\mathcal{M}$  given in Crutcher (1999); the values are given in Table 3. We find that  $\mathcal{M} \approx (1/2)\mathcal{T} \approx (1/4)\mathcal{W}$ , again indicating that magnetic fields are a significant, but not the sole, means of support against gravitational collapse. Finally, we find that  $2\mathcal{T} + \mathcal{M} = 1.3\mathcal{W}$ ; however, the surface pressure term in the virial equation, which is not included here, will act in the same sense as gravity; therefore, S88B is in approximate virial equilibrium.

## 5. CONCLUSIONS

We have observed OH thermal lines in absorption at 1665 and 1667 MHz toward the star forming region S88B with the aim of mapping magnetic fields via the Zeeman effect. The OH absorption line profiles toward this source are complicated, and contain several blended components toward a number of positions. The OH absorbing gas is located in the eastern parts of S88B, toward S88B-2 and the eastern section of S88B-1. The ratio of optical depths  $\tau_{67}/\tau_{65} = 1.0 - 1.3$  over most parts of the source, instead of the value of 1.8 for thermalized and homogenous OH gas. This is most likely due to clumping of OH gas, a conclusion supported by observations of CO,  $^{13}\text{CO}$ ,  $\text{NH}_3$  and  $\text{C}^{18}\text{O}$  emission lines from the literature. From the  $N(\text{OH})/T_{\text{ex}}$  plots, we identified 4 prominent OH clumps, which we have designated as OH-a, OH-b, OH-c, and OH-d. The highest values for  $N(\text{OH})/T_{\text{ex}}$  are to the north of the continuum peak S88B-2. Although this could, in principle, be due to an enhancement in  $N(\text{OH})$  or  $T_{\text{ex}}$  (or both), it is likely that north of S88B-2 is truly the location of the largest column of absorbing OH gas, as supported by independently measured extinction values toward S88B from the literature. Based on the observed quantities and adopted values of parameters from the literature, we obtain a gas density  $n(\text{H}_2) = 1.7 \times 10^5 \text{ cm}^{-3}$ , which compares well with the value of  $n(\text{H}_2) = 1.5 \times 10^5 \text{ cm}^{-3}$  found by Saito et al. (2007) for a  $\text{C}^{18}\text{O}$  clump coincident with the S88B-1 and S88B-2 sources.

In brief, S88B appears to have an overall geometry similar to M17, in that there is

an edge-on progression from ionized to molecular gas going eastward. Our magnetic field map appears to mirror this transition, at least over the extended S88B-1 region, where we detected line-of-sight magnetic fields ranging from 90-400  $\mu\text{G}$ , with the lowest values to the southwest of the S88B-1 continuum peak, and the highest values to its northeast. Toward S88B-2, the fields are significant at the  $3\text{-}\sigma$  level in the 1665 MHz line only, and are detected over a small region but if we had the sensitivity to keep going eastward, the field would likely follow the same increasing trend.

The detected fields allow us to assess the importance of the magnetic field in S88B, using a number of methods. We find that the ratio of thermal to magnetic pressures,  $\beta_p = 0.14$ ; a value of  $\beta_p < 1$  means that magnetic fields are important; the lower the value of  $\beta_p$ , the more dominant the magnetic field. A second method to assess the importance of the magnetic field is to compare the observed magnetic field with the critical field that would be required to completely support the cloud against its self-gravity. We find that the observed magnetic field is within a factor of 2 less than the critical field. A third method to assess the importance of the magnetic field, equivalent to the second, is to find the ratio of observed mass to magnetic flux in terms of the critical value; for S88B, we find this to be 1.8. These considerations lead us to conclude that the magnetic field in S88B is dynamically significant, and provides an important source of support against gravity. Moreover, the magnetic energy density is comparable to the turbulent energy density, implying that these two energies are in approximate equipartition, and pointing again to the importance of the magnetic field in this region.

This work has been partially supported by a Cottrell College Science Award (CCSA) grant from Research Corporation to A.P.S., and by start-up funds to A.P.S. at DePaul University. T.H.T. acknowledges NSF grant AST 03-07642. We thank Kaisa Young (*nee* Mueller) and H. Saito for sending us digital versions of their data for comparison. We have used extensively the NASA Astrophysics Data System (ADS) astronomy abstract service, the astro-ph web server, and the SIMBAD database.

## REFERENCES

- Boss, A. P. 2007, *ApJ*, 658, 1136
- Brogan, C. L., & Troland, T. H. 2001, *ApJ*, 560, 821
- Chini, R., Kreysa, E., Mezger, P. G., & Gemuend, H.-P. 1986, *A&A*, 154, L8
- Crutcher, R. M. 1977, *ApJ*, 216, 308
- Crutcher, R. M. 1979, *ApJ*, 234, 881
- Crutcher, R. M., Troland, T. H., & Kazes, I. 1987, *A&A*, 181, 119
- Crutcher, R. M. 1999, *ApJ*, 520, 706
- Deharveng, L., & Maucherat, M. 1978, *A&A*, 70, 19
- Deharveng, L., Nadeau, D., Zavagno, A., & Caplan, J. 2000, *A&A*, 360, 1107
- Evans, N. J., II, Harvey, P., Israel, F., Scholtes, M., de Graauw, T., Blair, G. N., Peters, W. L., III, & vanden Bout, P. 1981, *ApJ*, 250, 200
- Felli, M., & Harten, R. H. 1981, *A&A*, 100, 42
- Garay, G., Rodriguez, L. F., Moran, J. M., & Churchwell, E. 1993, *ApJ*, 418, 368
- Garay, G., Lizano, S., & Gomez, Y. 1994, *ApJ*, 429, 268
- Goetz, J. A., Gutermuth, R., Pipher, J. L., Forrest, W. J., & Howard, E. M. 2003, *ApJ*, 599, 1173
- Gomez, Y., Garay, G., & Lizano, S. 1995, *ApJ*, 453, 727
- Heiles, C., Goodman, A. A., McKee, C. F., & Zweibel, E. G. 1993, in *Protostars and Planets III*, ed. E. H. Levy & J. I. Lunine (Tucson: Univ. Arizona Press), 279
- Herter, T., Helfer, H. L., Briotta, D. A., Jr., Forrest, W. J., Houck, J. R., Rudy, R. J., Willner, S. P., & Pipher, J. L. 1982, *ApJ*, 262, 153
- Jourdain de Muizon, M., Cox, P., & Lequeux, J. 1990, *A&AS*, 83, 337
- Kazes, I., & Crutcher, R. M. 1986, *A&A*, 164, 328
- McKee, C. F., Zweibel, E. G., Goodman, A. A., & Heiles, C. 1993, in *Protostars and Planets III*, ed. E. H. Levy & J. I. Lunine (Tucson: Univ. Arizona Press), 327



- McKee, C. F. 1999, in *The Origin of Stars and Planetary Systems*, ed. C. J. Lada & N. D. Kylafis (Dordrecht: Kluwer), 29
- Mellon, R. R., & Li, Z.-Y. 2009, *ApJ*, 698, 922
- Mouschovias, T. C. 1987, in *Physical Processes in Interstellar Clouds*, ed. G. E. Morfill & M. Scholer (Dordrecht: Reidel), 453
- Mouschovias, T. C., Tassis, K., & Kunz, M. W. 2006, *ApJ*, 646, 1043
- Mozurkewich, D., Schwartz, P. R., & Smith, H. A. 1986, *ApJ*, 311, 371
- Mueller, K. E., Shirley, Y. L., Evans, N. J., II, & Jacobson, H. R. 2002, *ApJS*, 143, 469
- Nakamura, F., & Li, Z.-Y. 2005, *ApJ*, 631, 411
- Phillips, J. P., et al. 1988, *A&A*, 190, 289
- Phillips, J. P., & Mampaso, A. 1991, *A&AS*, 88, 189
- Pipher, J. L., Sharpless, S., Varlese, S., Savedoff, M. P., Krassner, J., Soifer, B. T., & Zeilik, M., II 1977, *A&A*, 59, 215
- Puga, E., Alvarez, C., Feldt, M., Henning, T., & Wolf, S. 2004, *A&A*, 425, 543
- Reifenstein, E. C., Wilson, T. L., Burke, B. F., Mezger, P. G., & Altenhoff, W. J. 1970, *A&A*, 4, 357
- Ridge, N. A., & Moore, T. J. T. 2001, *A&A*, 378, 495
- Roberts, D. A., Crutcher, R. M., & Troland, T. H. 1995, *ApJ*, 442, 208
- Saito, H., Saito, M., Sunada, K., & Yonekura, Y. 2007, *ApJ*, 659, 459
- Sarma, A. P., Troland, T. H., Roberts, D. A., & Crutcher, R. M. 2000, *ApJ*, 533, 271
- Sault, R. J., Killeen, N. E. B., Zmuidzinas, J., & Loushin, R. 1990, *ApJS*, 74, 437
- Sewilo, M., Watson, C., Araya, E., Churchwell, E., Hofner, P., & Kurtz, S. 2004, *ApJS*, 154, 553
- Shu, F. H., Galli, D., Lizano, S., & Cai, M. 2006, *ApJ*, 647, 382
- Troland, T. H., & Heiles, C. 1982, *ApJ*, 252, 179
- White, G. J., & Fridlund, C. V. M. 1992, *A&A*, 266, 452

Wood, D. O. S., & Churchwell, E. 1989, *ApJS*, 69, 831

Wu, Y., & Evans, N. J., II 1989, *ApJ*, 340, 307

Zhao, B., Li, Z.-Y., Nakamura, F., Krasnopolsky, R., & Shang, H. 2011, *ApJ*, 742, 10

Zinnecker, H., & Yorke, H. W. 2007, *ARA&A*, 45, 481

Table 1. PARAMETERS FOR VLA OBSERVATIONS

Parameter	B-configuration	C-configuration
Date	2003 Nov 28/29, Dec 1/2	1997 Aug 15/16
Configuration	B	C
R.A. of field center (J2000)	$19^h46^m47^s.7$	$19^h46^m47^s.7$
Decl. of field center (J2000)	$25^\circ12'56''.1$	$25^\circ13'05''.2$
Total bandwidth (MHz)	0.20	0.20
No. of channels	128	128
Channel Spacing ( $\text{km s}^{-1}$ )	0.28	0.28
Approx. time on source (hr)	6.7	8.9
Rest frequency (MHz)	1665.402	1665.402
	1667.359	1667.359

Note. —  $1' = 0.6$  pc, for adopted distance to S88B = 2.0 kpc (see § 1.1)

Table 2. Source Parameters

Parameter	Value
Radius ( $r$ )	0.2 pc
Column Density ( $N_{\text{H}_2}$ )	$7.2 \times 10^{22} \text{ cm}^{-2}$
Particle Density ( $n_{\text{p}}$ )	$1.7 \times 10^5 \text{ cm}^{-3}$
Kinetic Temperature ( $T_{\text{k}}$ )	60 K
Adopted Average FWHM Linewidth ( $\Delta v$ )	$2.5 \text{ km s}^{-1}$
Average Magnetic Field ( $B_{\text{los}}$ )	$200 \mu\text{G}$

Table 3. Source A : Derived Values and Virial Estimates

Parameter	Value
$m_s$	4.0
$m_A$	1.0
$\beta_p$	0.14
$[M/\Phi_B]_{\text{obs/crit}}$	1.8
$\mathcal{W}$	$1.3 \times 10^{46}$ ergs
$\mathcal{T}/\mathcal{W}$	0.54
$\mathcal{M}/\mathcal{W}$	0.22

Note. —  $m_s$  is the sonic Mach number equal to  $\sqrt{3}\sigma/c_s$ , where  $\sigma$  is the line velocity dispersion and  $c_s$  is the speed of sound;  $m_A$  is the Alfvénic Mach number equal to  $\sqrt{3}\sigma/v_A$ , where  $v_A$  is the Alfvén velocity,  $\beta_p$  is the ratio of thermal to magnetic pressures,  $M/\Phi_B$  is the mass to magnetic flux ratio,  $\mathcal{W}$  is the virial gravitational energy,  $\mathcal{T}$  is the virial kinetic energy, and  $\mathcal{M}$  is the virial magnetic energy; expressions for calculating all these terms were taken from Crutcher (1999).

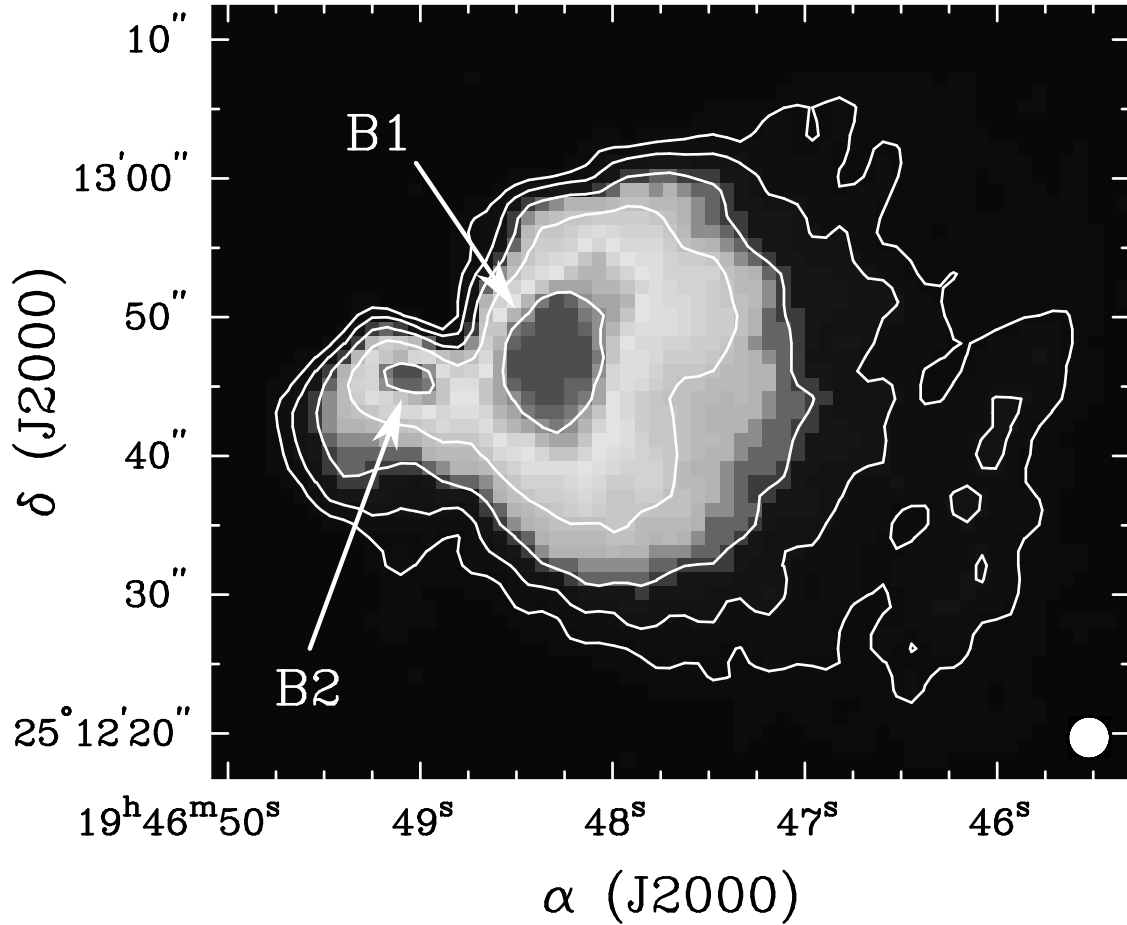


Fig. 1.— Contour image of the 18 cm continuum toward S88B. The beam is  $3''.1 \times 3''.0$  (P.A. $=-6^\circ.1$ ), and the rms in the image is  $0.8 \text{ mJy beam}^{-1}$ . The contours are at 6, 12, 24, 48, 96  $\text{mJy beam}^{-1}$ . The extended western component S88B-1, and the compact component to the east S88B-2, are marked in the figure as B1 and B2 respectively.



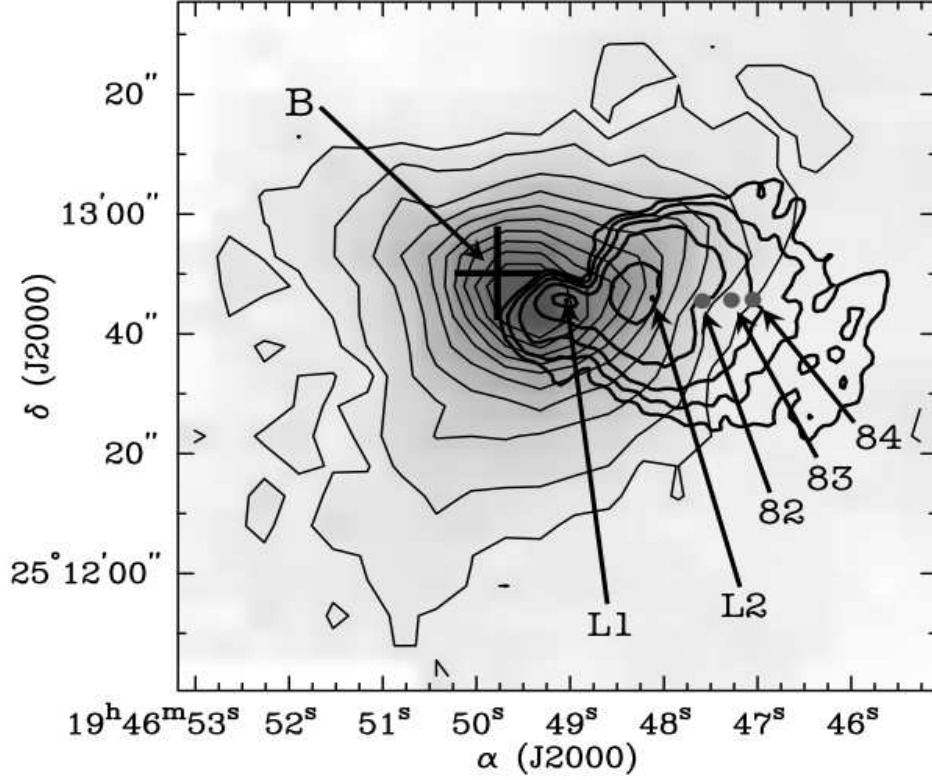


Fig. 2.— Contours and grayscale of the  $350 \mu\text{m}$  dust emission toward S88B from Mueller et al. (2002) superposed on the 18 cm continuum image. The HPBW of the  $350 \mu\text{m}$  data is  $14''$ , and contours are at  $1.4, 2 \text{ Jy beam}^{-1}$ , and then in increments of  $1 \text{ Jy beam}^{-1}$  up to  $10 \text{ Jy beam}^{-1}$ . Our 18 cm continuum image has the same resolution and contours as in Figure 1. The positions of the NIR sources 82, 83, and 84 from Deharveng et al. (2000), the  $3.5 \mu\text{m}$  sources L1 and L2 from Puga et al. (2004), and clump B from the  $\text{C}^{18}\text{O}$  observations of Saito et al. (2007) are also marked in the figure.

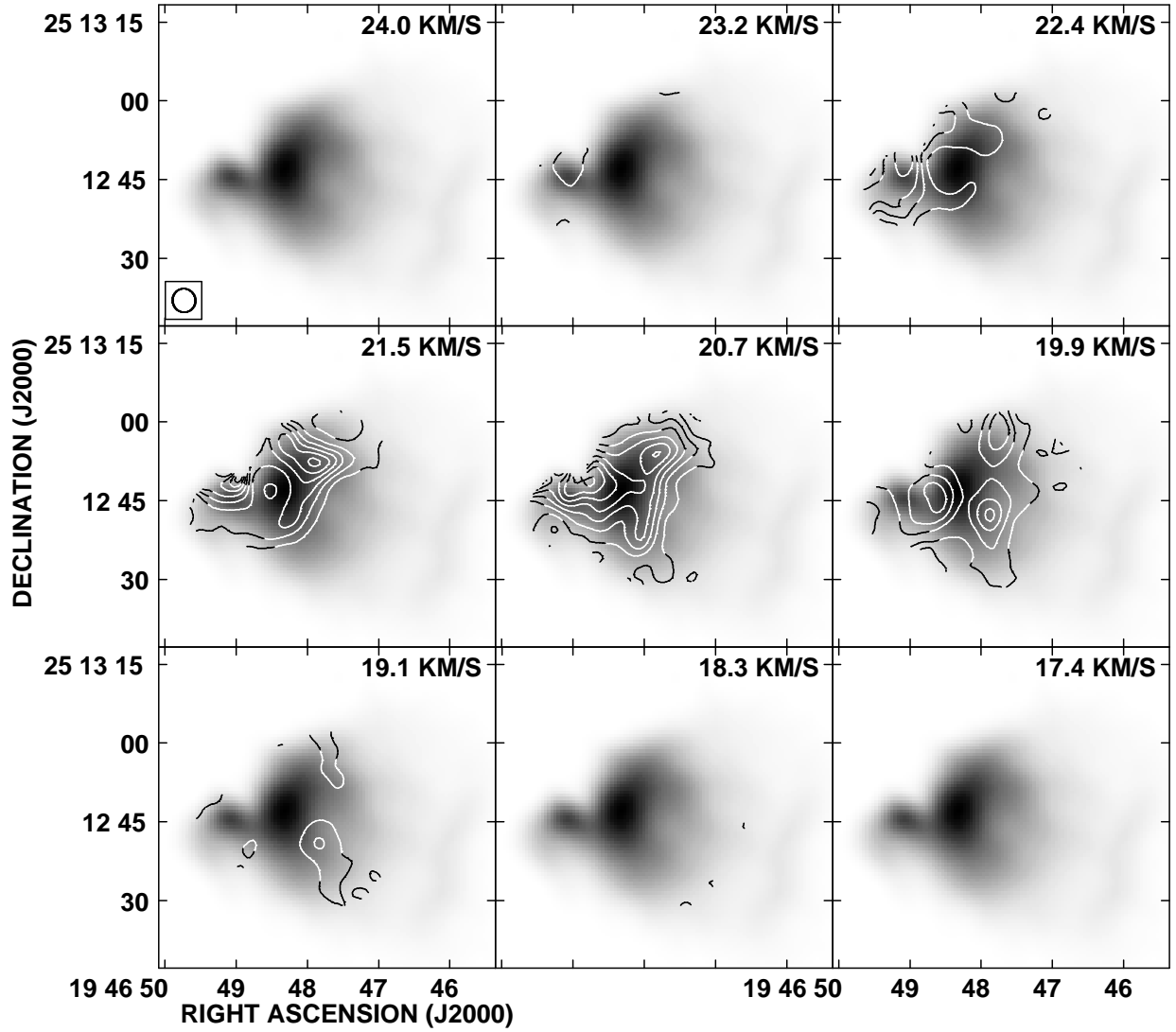


Fig. 3.— OH 1667 MHz optical depth channel images from  $17.4 \text{ km s}^{-1}$  to  $24.0 \text{ km s}^{-1}$  in  $v_{\text{LSR}}$ . The contours are from  $\tau = 0.25$  to  $\tau = 2.0$  in steps of 0.25. Every third velocity channel is displayed. The grayscale shows the 18 cm continuum at the same resolution as the OH optical depth image, which is  $4''.5 \times 4''.3$  (P.A.= $14^\circ 1$ ), as shown in the boxed inset in the top left panel.

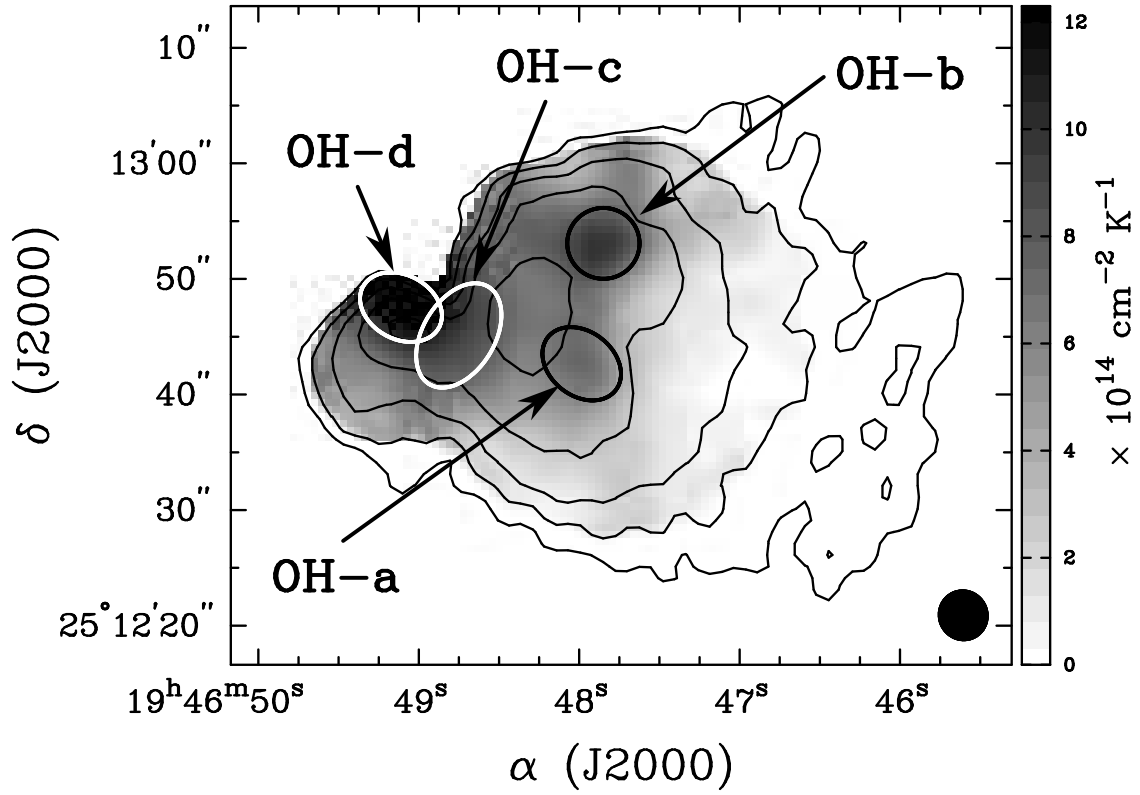


Fig. 4.— Gray-scale image of  $N_{\text{OH67}}/T_{\text{ex}}$  toward S88B overlaid on the 18 cm continuum. The continuum image has the same resolution and contours as in Fig. 1. The 1667 OH beam is shown in the lower right; its parameters are given in Fig. 3.

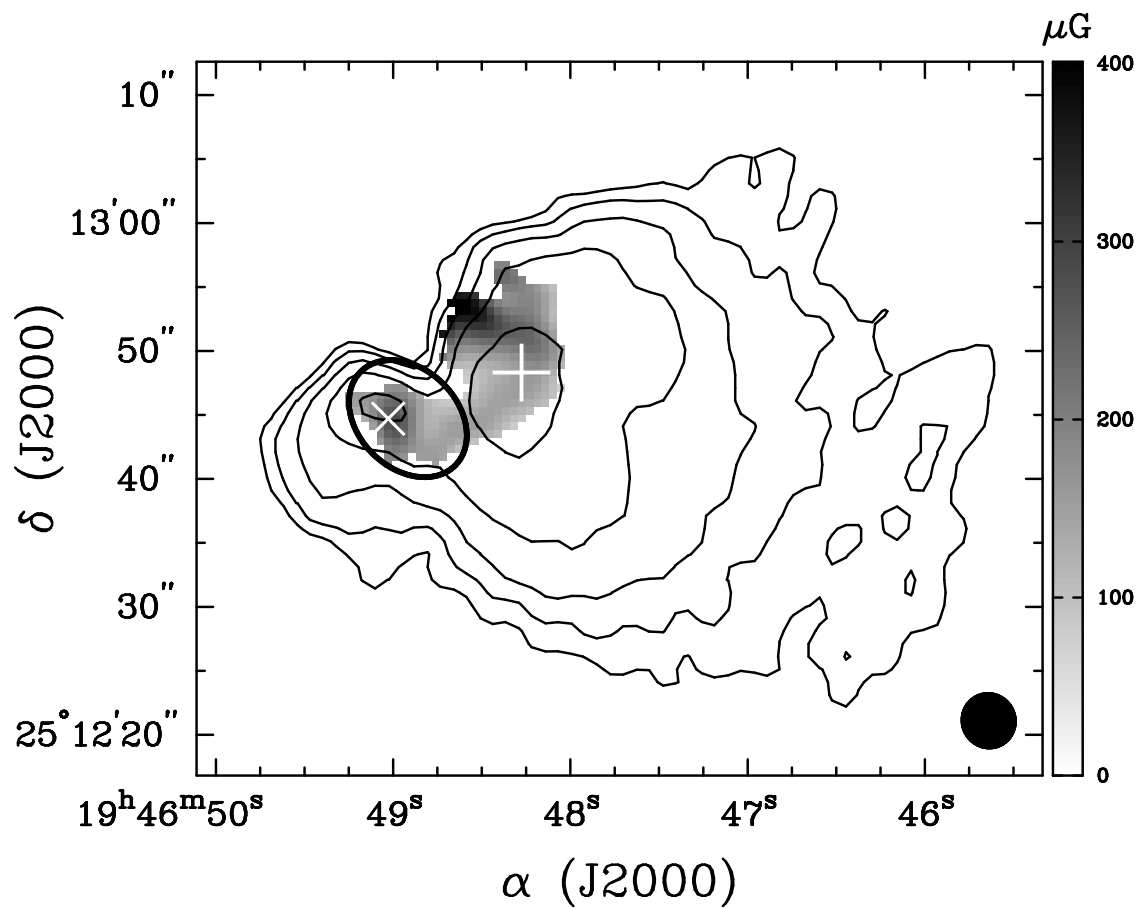


Fig. 5.— Image of the detected  $B_{\text{los}}$  toward S88B, taken from the 1665 MHz data. The contours depict the 18 cm continuum, and are the same as in Fig 1. The thick-lined ellipse shows the region in which the detected  $B_{\text{los}}$  is at the  $3\text{-}\sigma$  level in 1665 MHz only. The “+” sign indicates the position toward which the profiles are shown in Fig. 6 below, while the “x” indicates the position toward which the profiles are shown in Fig. 7.

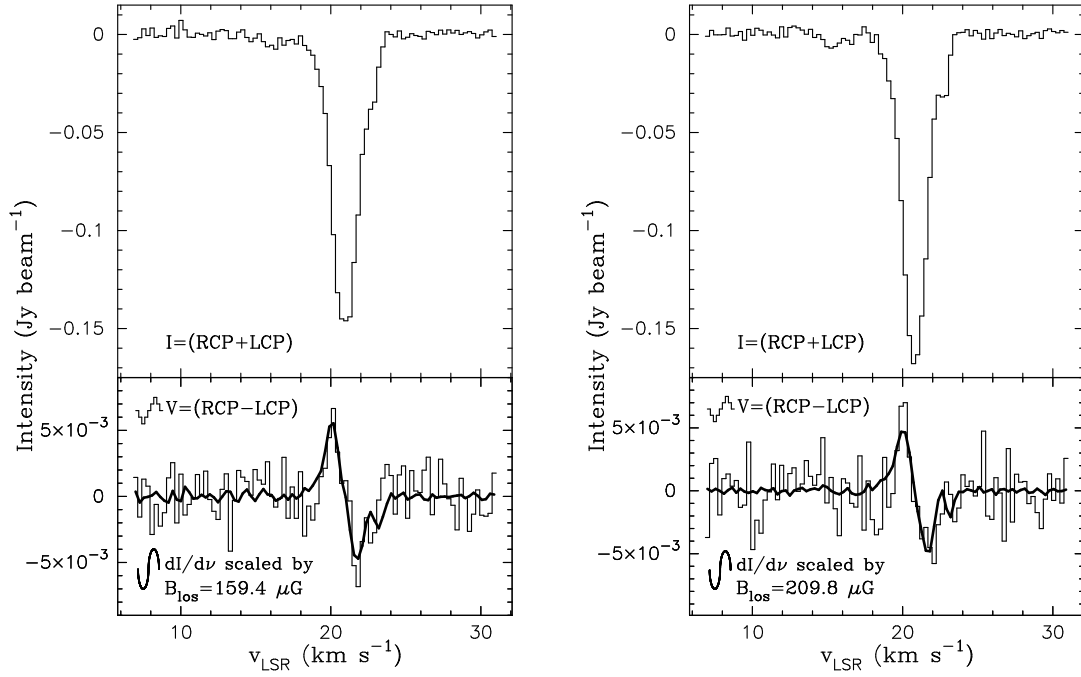


Fig. 6.— Stokes  $I$  (top; histogram) and  $V$  (bottom; histogram) profiles at 1665 MHz (left) and 1667 MHz (right) toward the position in S88B-1 marked in Fig. 5 by a “+” ( $\alpha_{2000} = 19^{\text{h}}46^{\text{m}}48^{\text{s}}.3$ ,  $\delta_{2000} = 25^{\circ}12'48''.3$ ). The curve superposed on  $V$  in the lower frame on the left shows the derivative of  $I$  at 1665 MHz scaled by  $B_{\text{los}} = 159.4 \pm 18.0 \mu\text{G}$ , whereas the curve superposed on  $V$  in the lower frame on the right shows the derivative of  $I$  at 1667 MHz scaled by  $B_{\text{los}} = 209.8 \pm 29.5 \mu\text{G}$ .

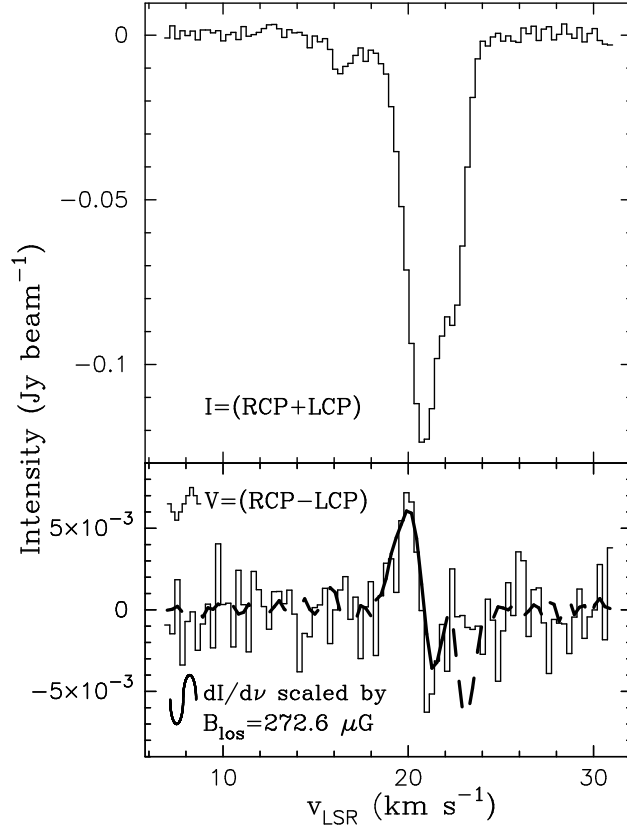


Fig. 7.— Stokes  $I$  (top; histogram) and  $V$  (bottom; histogram) profiles at 1665 MHz toward the position in S88B-2 marked in Fig. 5 by a “ $\times$ ” ( $\alpha_{2000} = 19^{\text{h}}46^{\text{m}}49^{\text{s}}.0$ ,  $\delta_{2000} = 25^{\circ}12'44''.7$ ). The curve superposed on  $V$  in the lower frame shows the derivative of  $I$  at 1665 MHz scaled by  $B_{\text{los}} = 272.6 \pm 40.7 \mu\text{G}$ ; the fit for the field was made over a restricted range of velocity channels, and the channels over which the fit was made are indicated by the solid line.